Lattice density-functional theory of the attractive Hubbard model

Matthieu Saubanère
Institut Charles Gerhardt, Centre National de la Recherche Scientifique, Université Montpellier, Place Eugène Bataillon, 34095 Montpellier, France

G. M. Pastor
Institut für Theoretische Physik, Universität Kassel, Heinrich Plett Straße 40, 34132 Kassel, Germany

(Received 21 November 2013; revised manuscript received 2 September 2014; published 17 September 2014)

The attractive Hubbard model is investigated in the framework of lattice density-functional theory (LDFT). The ground-state energy $E = T + W$ is regarded as a functional of the single-particle density matrix γ_{ij} with respect to the lattice sites, where $T[\gamma]$ represents the kinetic and crystal-field energies and $W[\gamma]$ the interaction energy. Aside from the exactly known functional $T[\gamma]$, we propose a simple scaling approximation to $W[\gamma]$, which is based on exact analytic results for the attractive Hubbard dimer and on a scaling hypothesis within the domain of representability of γ. As applications, we consider one-, two-, and three-dimensional finite and extended bipartite lattices having homogeneous or alternating onsite energy levels. In addition, the Bethe lattice is investigated as a function of coordination number. Results are given for the kinetic, Coulomb, and total energies, as well as for the density distribution γ_{ii}, nearest-neighbor bond order γ_{ij}, and pairing energy ΔE_p, as a function of the interaction strength $|U|/t$, onsite potential ε/t, and band filling $n = N_e/N_a$. Remarkable even-odd and super-even oscillations of ΔE_p are observed in finite rings as a function of band filling. Comparison with exact Lanczos diagonalizations and density-matrix renormalization-group calculations shows that LDFT yields a very good quantitative description of the properties of the model in the complete parameter range, thus providing a significant improvement over the mean-field approaches. Goals and limitations of the method are discussed.

DOI: 10.1103/PhysRevB.90.125128 PACS number(s): 71.10.Fd, 71.45.Lr, 71.27.+a

I. INTRODUCTION

The study of strong electron-correlation phenomena and in particular the description of pairing mechanisms leading to superconductivity remain a major challenge in solid-state physics. In conventional superconductors, pairing of electrons is known to be induced at the Fermi energy by an effective off-diagonal attractive interaction mediated by phonons. The physics behind this most remarkable many-body effect has been first explained by the theory of Bardeen, Cooper, and Schrieffer (BCS) [1]. An alternative approach to study the consequences of electronic pairing in metals is to consider the Hubbard model [2] with attractive local interactions [3,4]. The conceptual differences between the paring mechanisms in the BCS and Hubbard Hamiltonians could hardly be more profound. The BCS interaction is most clearly understood from a reciprocal k-space representation. It involves the scattering of pairs of electrons having nearly the same energy since the interaction is mediated by phonons, whose frequency cannot be larger than the Debye frequency ω_D. The narrow momentum dispersion $\hbar\Delta k$ caused by the interactions implies that the spatial extension Δr of the Cooper pairs is quite large. Actually, Δr is of the order of $1/\Delta k = v_F/\omega_D$, where $v_F = \hbar k_F/m^*$ refers to the Fermi velocity. In contrast, the Hubbard interaction is strictly local in real space. It involves pairs of electrons occupying the same lattice site with opposite spins. If regarded from a k-space perspective, the Hubbard interaction is equivalent to assuming that the scattering amplitude between pairs of electrons is independent of both the incoming momenta and the momentum transfer. It is therefore considerably interesting to investigate the attractive Hubbard model, in order to assess the properties resulting from such contrasting types of interactions.

Over the past years, several theoretical investigations of the physics of attractive local interactions have been performed [3–7]. The first ones have been focused on studying the phase diagram of the Hubbard model on lattices having different dimensions, hopping integrals, and band fillings [3]. A variety of complementary theoretical approaches have been used including weak and strong coupling methods and Monte Carlo simulations. In particular, the formation and stability of charge-density waves (CDWs) and superconducting states induced by local attractive interactions has been quantified [3]. Other works have addressed the accuracy of the mean-field BCS approximation for the attractive Hubbard model by comparing it with exact numerical calculation on finite and extended one- and two-dimensional (1D and 2D) lattices at different interaction regimes [4–6]. While the BCS approach has been shown to be an excellent approximation for the ground-state energy in general, it is less accurate for the energy gap. These studies have also revealed remarkable even-odd and super-even oscillations of the pairing energy as a function of the number of electrons in finite structures [5]. More recently, it has been shown that in highly disordered InO thin films, close to the superconductor-insulator transition, the Cooper pairs are spatially localized [8]. This effect is the result of the competition between single-particle disorder, which tends to localize the electronic states, and the formation of the spatially extended Cooper pairs responsible for the superconducting state [9]. The interplay between the static CDWs induced by random single-particle potentials and the dynamic paring correlations resulting from attractive local interactions is therefore of considerable interest [10]. The competition between single-particle localization and many-body correlations can be simulated by introducing site-dependent local energy levels in many-body lattice models.

The purpose of this paper is to investigate the inhomogeneous attractive Hubbard Hamiltonian in the framework of lattice density-functional theory (LDFT). This approach to the quantum many-body problem considers the single-particle density matrix γ_{ij} with respect to the lattice sites i and j as the central variable [11–14]. Based on a Hohenberg-Kohn–type theorem [15] for general lattice models [16], formal expressions have been obtained for the kinetic-energy functional $T[\gamma]$ and for the interaction-energy functional $W[\gamma]$ following Levy's constrained-search minimization [17]. In this way, the ground-state energy is regarded as a functional $E[\gamma] = T[\gamma] + W[\gamma]$ of the density matrix γ [11]. A variational scheme allows one to determine the ground state $E_{\rm gs}$ and $\gamma_{\rm gs}$ from the minimization of $E[\gamma]$. In contrast to the Hohenberg-Kohn-Sham density-functional theory (DFT) [15,18], which incorporates the correlation contributions to the kinetic and Coulomb energies through the so-called exchange and correlation functional $E_{\rm XC}[\rho(\vec{r})]$, LDFT uses a simple exact expression for the kinetic energy $T[\gamma]$ of the electrons in the lattice. However, as in the continuum, a closed explicit expression for the Coulomb-energy functional $W[\gamma]$ remains unknown. Approximations to W have been derived for the repulsive Hubbard model ($U > 0$) by using exact dimer results and by taking advantage of the scaling properties of $W[\gamma]$ within its domain of representability [12,14]. This ansatz has been subsequently extended to systems showing inhomogeneous charge distributions [19,20]. Applications of the method show very encouraging results in a variety of physical situations including finite and extended repulsive Hubbard models in one, two, and three dimensions [12], dimerized chains [13,14], and bipartite lattices with alternating onsite potentials [20,21].

The existing density-functional approaches to lattice models may be divided essentially in two groups. The first one uses the local site occupations n_i as basic variables of the many-body problem. This perspective has been originally proposed in order to investigate the band-gap problem in semiconductors [22]. The second group considers both the diagonal elements $\gamma_{ii} = n_i$ and the off-diagonal elements γ_{ij} of the single-particle density matrix as formulated in Ref. [23]. These two approaches have been contrasted by showing that different basic variables and different energy functionals may be considered depending on the type of model under study [24]. More recently, following these ideas, Lima *et al.* proposed a local approximation in terms of site occupations $n_i = \gamma_{ii}$ alone, which is based on exact Bethe-ansatz results for the one-dimensional (1D) Hubbard model [25,26]. This approach has been applied to describe strongly correlated systems far from equilibrium [27], the transport through an Anderson junction [28,29], and the band gap of the inhomogeneous Hubbard model [30]. However, the problem of electron delocalization throughout the lattice cannot be addressed by using these functionals since the basic variables are the local site occupations γ_{ii} alone. Moreover, it can be shown that these formulations are not universal in the sense that the corresponding functionals are not independent of the lattice structure. These restrictions do not apply to functionals which take into account the off-diagonal components γ_{ij} of the density matrix. Among the latter density-matrix approaches one should mention the developments of Carlsson and co-workers [31,32]. These authors proposed a performant exchange-correlation functional for the Hubbard model by interpolating between well-established limits, as well as an implicit energy functional for the Anderson model based on a rigorous inequality for the interaction energy. A further approach to the Anderson model has been developed in the context of lattice density-functional theory [16].

In order to apply LDFT to the attractive Hubbard model, it is necessary to find an explicit approximation to the interaction-energy functional $W[\gamma]$, which correctly describes the correlations leading to electronic pairing. This is a most interesting issue from both methodological and practical perspectives. On the one side, from the point of view of the many-body problem, it is important to understand the functional dependence of $W[\gamma]$ for attractive couplings and to compare its behavior with the far more intensively studied repulsive case. Coulomb repulsion stabilizes uniform charge distributions and tends to block local charge fluctuations associated to the interatomic hoppings, delocalization, and band formation. It favors the development of local magnetic moments $\langle S_i^2 \rangle$, which adopt low-spin antiferromagnetic arrangements or high-spin ferromagnetic order depending on band filling and interaction strength [33–37]. In contrast, attractive interactions favor electronic pairing and vanishing local moments at all lattice sites. The kinetic energy operator (i.e., electronic hopping) tends here to break pair formation thereby enhancing $\langle S_i^2 \rangle$. For $U > 0$, small values of the off-diagonal density-matrix elements γ_{ij} correspond to small W (i.e., weak charge fluctuations) while for $U < 0$, small γ_{ij} correspond to the strongest pairing and the largest $|W|$. On the other side, from a physical perspective, it is challenging to elucidate the properties of correlated attracting fermions. LDFT provides us with an alternative viewpoint to this interesting problem. Moreover, taking into account the very good accuracy of the method in studies of the repulsive model [12–14,20], it is reasonable to expect that it should also be effective for $U < 0$, and that it should give a new insight into the attractive many-body problem.

The reminder of the paper is organized as follows. In Sec. II, the basic background on LDFT is recalled, giving emphasis to the details concerning the $U < 0$ case. The properties of the exact interaction-energy functional $W[\gamma]$ are investigated in Sec. III. First, we analyze exact results for $W[\gamma]$, which were obtained by performing Levy-Lieb's constrained minimization numerically on 1D and 2D clusters with periodic boundary conditions. The scaling properties of W within the domain of representability of γ are thereby demonstrated. As a result, we derive a simple explicit approximation to W, which is based on the exact solution of the two-site problem and a scaling hypothesis. In Sec. IV, the theory is applied to the attractive Hubbard model on 1D and 2D bipartite lattices. The ground-state properties and pairing energies are discussed as a function of the model parameters. Quantitative comparisons are made between LDFT and other available methods, such as Lanczos [38], density-matrix renormalization group (DMRG) [39], and BCS approximation [4,5], in order to assess goals and limitations of our approach. Finally, Sec. V summarizes our conclusions.

II. THEORETICAL METHOD

The general formulation of LDFT is for the most part independent of the nature of the interactions [11–14,19,20]. However, the properties of the central interaction-energy functionals are model specific. It is therefore worth to discuss the method from the perspective of the attractive Hubbard model. We consider the Hamiltonian [2]

$$\hat{H} = \sum_{i,\sigma} \varepsilon_i \hat{n}_{i\sigma} + \sum_{\langle i,j\rangle\sigma} t_{ij} \hat{c}^{\dagger}_{i\sigma} \hat{c}_{j\sigma} + U \sum_{i} \hat{n}_{i\downarrow} \hat{n}_{i\uparrow}, \qquad (1)$$

where ε_i denotes the site-dependent energy levels, t_{ij} the nearest-neighbor (NN) hopping integrals, and U the onsite interaction. As usual, $\hat{c}^{\dagger}_{i\sigma}$ ($\hat{c}_{i\sigma}$) stands for the creation (annihilation) operator for an electron with spin σ at site i ($\hat{n}_{i\sigma} = \hat{c}^{\dagger}_{i\sigma}\hat{c}_{i\sigma}$). The hopping elements t_{ij} define the structure and dimensionality of the lattice, as well as the range of the single-particle hybridizations. The energy levels ε_i describe the arrangement of different elements in the lattice or the effects of external fields. The parameters ε_i and t_{ij} specify the system under study, and thus play the role of the external potential $v_{\rm ext}(\vec{r})$ in conventional DFT. Consequently, the basic variable in a density-functional theory of lattice models is the single-particle density matrix γ_{ij} with respect to the sites i and j. Notice that this involves not only the diagonal elements γ_{ii}, which describe merely the charge distribution, but also the off-diagonal elements or bond orders γ_{ij}, which give a measure of the degree of electron delocalization.

The ground-state energy $E_{\rm gs}$ and density matrix $\gamma^{\rm gs}_{ij}$ are determined by minimizing the energy functional

$$E[\gamma] = T[\gamma] + W[\gamma] \qquad (2)$$

with respect to γ_{ij}. $E[\gamma]$ is defined for all density matrices that derive from a physical state, i.e., that are given by

$$\gamma_{ij} = \sum_{\sigma} \gamma_{ij\sigma} = \sum_{\sigma} \langle \Psi | \hat{c}^{\dagger}_{i\sigma} \hat{c}_{j\sigma} | \Psi \rangle, \qquad (3)$$

where $|\Psi\rangle$ is an N-fermion state. Density matrices satisfying the previous equation are said to be pure-state N-representable since they derive from well-defined N-electron states [40]. In this context it is useful to distinguish the more restrictive set of pure-state interacting v-representable γ_{ij}, sometimes simply denoted as v-representable γ_{ij}. This is given by the density matrices that derive from a *ground state* of Eq. (1). In other words, a v-representable γ_{ij} is equal to $\gamma^{\rm gs}_{ij}$ for some values of the model parameters ε_i, t_{ij}, and U. Obviously, all v-representable γ are N-representable. However, the converse is not always true [11].

The single-particle contributions to the energy are given by

$$T[\gamma] = \sum_{i} \varepsilon_i \gamma_{ii} + \sum_{i \neq j} t_{ij} \gamma_{ij}. \qquad (4)$$

The first term in Eq. (4) is the charge-distribution (CD) energy $E_{\rm CD}[\gamma_{ii}]$, which depends only on the diagonal elements of γ. The second one is the kinetic energy $E_{\rm K}[\gamma_{ij}]$ associated with the delocalization of the electrons in the lattice, which depends on the off-diagonal elements of γ for which $t_{ij} \neq 0$, typically the NN ij. Notice that no approximation is involved in the functional dependencies of $E_{\rm CD}$ and $E_{\rm K}$. Thus, the effects of correlations on the single-particle energy $T[\gamma]$ are taken into account exactly.

The interaction-energy functional can be written as

$$W[\gamma] = \min_{\Psi \to \gamma} \left[U \sum_{i} \langle \Psi[\gamma] | \hat{n}_{i\uparrow} \hat{n}_{i\downarrow} | \Psi[\gamma] \rangle \right], \qquad (5)$$

where the minimization runs over all N-particle states $|\Psi\rangle$ yielding the given γ [11]. The N-representability condition (3) ensures that the minimization domain is not empty. This approach, known as constrained-search minimization, was first proposed for the continuum [17]. The condition that $|\Psi\rangle$ yields γ (i.e., $\langle \Psi | \hat{c}^{\dagger}_{i\sigma} \hat{c}_{j\sigma} | \Psi \rangle = \gamma_{ij\sigma}$) separates the ensemble of all physical states in disjoint equivalence classes or representing sets, one for each γ. It is important to observe that the internal structure and composition of these classes, although crucial for the functional dependence of $W[\gamma]$, is completely independent of the nature of the many-body interactions. As the Hilbert space containing all $|\Psi\rangle$, the representing sets depend only on the number of electrons N_e and the number of atoms or sites N_a. A universal relation between γ and the states that represent it also holds between ensemble-representable γ and mixed states. It is of course the minimum value attained by the interaction energy within each representing set what depends on the type of coupling. The notion of v-representability is, however, model and even system dependent.

For attractive interactions ($U < 0$), the functional $W[\gamma]$ represents the maximum value of the average number of double occupations that is compatible with a given density matrix γ, the latter fixing the charge distribution and the degree of electron delocalization. W is universal in the sense that it is independent of the system under study, which is defined by the external parameters ε_i and t_{ij}. However, W depends on the internal structure of the many-body Hilbert space, as defined by the number of electrons $N_e = \sum_i \gamma_{ii}$ and the number of atoms or sites N_a. It is also depends, of course, on the operator describing the interactions, in the present case the attractive onsite model.

In this context, it is interesting to analyze the dependence of $W[\gamma]$ on the interaction parameter U since this reveals rigorous constraints to be satisfied by any explicit approximation. Once the sign of U is defined, it is clear that the minimization in Eq. (5) is independent of $|U|$ since the representability constraints are independent of U. Therefore, we may write

$$W[\gamma] = -|U| \max_{\Psi \to \gamma} \left[\sum_{i} \langle \Psi[\gamma] | \hat{n}_{i\uparrow} \hat{n}_{i\downarrow} | \Psi[\gamma] \rangle \right] \qquad (6)$$

for all $U < 0$. A strict linearity of $W[\gamma]$ as a function of U follows. This important property is a consequence of the fact that the density matrix γ univocally defines all single-particle contributions. The situation is different in the DFT of the continuum since the electronic density $n(\vec{r})$ is not enough to define the kinetic energy unambiguously. In this case, the Hohenberg-Kohn or Levy-Lieb functionals reflect the compromise of minimizing the sum $T + W$ of the kinetic and interaction energies for a given $n(\vec{r})$.

Finally, the variational principle for the ground-state density matrix $\gamma^{\rm gs}_{ij}$ follows from the relations [17]

$$E_{\rm gs} \leqslant E[\gamma] = T[\gamma] + W[\gamma] \qquad (7)$$

for all pure-state N-representable γ and

$$E_{\rm gs} = T[\gamma^{\rm gs}] + W[\gamma^{\rm gs}], \tag{8}$$

where $E_{\rm gs} = \langle\Psi_{\rm gs}|\hat{H}|\Psi_{\rm gs}\rangle$ is the ground-state energy. The present formulation of LDFT can be generalized to arbitrary forms of the two-body interaction $V_{ijkl}\hat{c}^{\dagger}_{i,\sigma}\hat{c}^{\dagger}_{j,\sigma'}\hat{c}_{k,\sigma'}\hat{c}_{l,\sigma}$, for example, to site-dependent Hubbard-type interactions or Anderson impurity models [13,16].

III. INTERACTION-ENERGY FUNCTIONAL FOR ATTRACTIVE INTERACTIONS

The purpose of this section is to explore the interaction energy W of the attractive Hubbard model as a function of the single-particle density matrix γ and to derive an explicit approximation to $W[\gamma]$, which is suitable for general applications. First, the domain of representability of γ is analyzed. Second, exact results for $W[\gamma]$ are derived by implementing Levy-Lieb's constrained search numerically using the Lanczos method [38]. Finally, the scaling properties of W are demonstrated, on the basis of which a scaled dimer approximation is proposed.

A. Representability domain of γ

Before discussing the properties of W for attractive interactions, it is useful to examine the representability domain of γ. Figure 1 shows the NN bond order γ_{12} as a function of the sublattice occupation number γ_{11}, in the ground state of a 1D Hubbard chain having $N_a = 14$ sites, band filling $n = 1$, and alternating energy levels $\varepsilon_i = \pm\varepsilon/2$. The curves are symmetric with respect to the homogeneous case ($\gamma_{11} = \gamma_{22}$) since $(\gamma_{11} + \gamma_{22})/2 = n = 1$. The results display the correlation between diagonal and off-diagonal elements

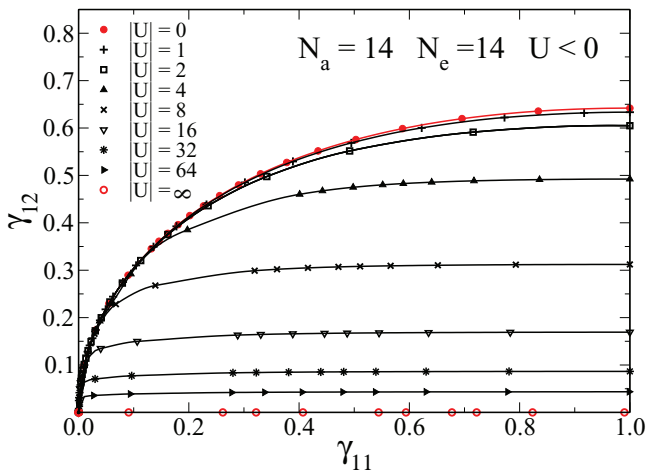

FIG. 1. (Color online) Correlation between the NN bond order γ_{12} and the average sublattice occupation γ_{11} in the ground state of a 1D attractive Hubbard chain having alternating energy levels $\varepsilon_i = \pm\varepsilon/2$, $N_a = 14$ sites, and half-band filling $n = 1$. Different values of the local interaction $U < 0$ are considered as indicated. The region enclosed by the upper bound γ^0_{12} (red curve, full circles, $U = 0$) and the lower bound $\gamma^{\infty}_{12} = 0$ (open circles, $U = -\infty$) defines the domain of representability of γ.

of the density matrix, as derived from the ground state of the model for different values of the energy-level difference ε, NN hopping t, and interaction strength $|U|$. These v-representable γ include all the ground state $\gamma^{\rm gs}$, which are in one-to-one correspondence with a many-body ground state $|\Psi_{\rm gs}\rangle$ [16]. Aside from $\gamma^{\rm gs}$, it is also important to investigate the properties of the more general N-representable γ, which constitute the domain of definition of Levy's functional $W[\gamma]$.

For each γ_{11}, or charge transfer $\Delta n = \gamma_{22} - \gamma_{11}$, the upper bound γ^0_{12} for the NN γ_{12} corresponds to the largest possible value of the kinetic energy. This is achieved by the uncorrelated ground state for the given Δn. In most cases, the underlying electronic state is a single Slater determinant and therefore the interaction energy coincides with the Hartree-Fock energy $W^0 = W[\gamma^0] = UN_a(\gamma^2_{11} + \gamma^2_{22})/8$. This does not hold in the presence of degeneracies at the Fermi energy of the single-particle spectrum, in which case a multideterminant ground state cannot be avoided even for $U \to 0$ (e.g., for $N_a = N_e = 4$ and $\Delta n = 0$). The uncorrelated γ^0_{12} is largest for a homogeneous density distribution ($\Delta n = 0$) and decreases monotonically as the charge transfer increases. It vanishes in the limit where only one sublattice is occupied (see Fig. 1). This can be understood by recalling that in an uncorrelated state, an increase of Δn corresponds to an increase of the energy-level difference ε between the sublattices, which reduces the degree of electron delocalization γ_{12}. In the limit of complete charge transfer ($\gamma_{11} \to 0$), no charge fluctuations are possible at all.

The noninteracting curve in Fig. 1 encloses the v-representable domain. For $\gamma_{12} < \gamma^0_{12}$, and a given Δn, there is a larger flexibility in the states representing γ. Therefore, the electronic system can reduce the interaction energy $W[\gamma]$ for the given γ_{ij} by increasing the average number of double occupations $\omega = W/UN_a$, as required by the Levy-Lieb constrained minimization. Its largest possible value is $\omega^{\infty} = W^{\infty}/UN_a = N_e/2N_a$ for N_e even, and $\omega^{\infty} = (N_e - 1)/2N_a$ for N_e odd. The largest and thus optimal value of γ_{12} yielding the $W = W^{\infty}$ is denoted by γ^{∞}_{12}. It defines the lower bound of the v-representable domain of γ_{12} and corresponds to the ground state of the model for $U \to -\infty$, where $W(\gamma^{\infty}_{12}) = W^{\infty}$ (see Fig. 1). For N_e even, all electrons can be paired and therefore $\gamma^{\infty}_{ij} = 0$. However, for N_e odd, an unpaired electron remains, which yields a finite γ^{∞}_{12}. This contribution can be important for calculating properties of finite systems which involve changes in the number of electrons (e.g., the pairing energy). As expected, the N-representable domain, being independent of the type of interaction, is the same as in the repulsive case. However, the interacting v-representable domains are different (see also Ref. [19]).

B. Scaling properties of $W[\gamma]$

In Fig. 2(a), exact results for W are shown as a function of γ_{12} for representative values of $\Delta n = \gamma_{22} - \gamma_{11}$. These were obtained by solving Eq. (6) for a ring having $N_a = 14$ sites and half-band filling $n = N_e/N_a = 1$. The most interesting correlation-energy functional $E_c = W - E_{\rm HF}$ is highlighted in Fig. 2(b). Despite the strong dependence of W on Δn, there are several important qualitative features, which are shared by all the curves: (i) As already discussed, the domain of N-representability of γ_{12} is delimited by

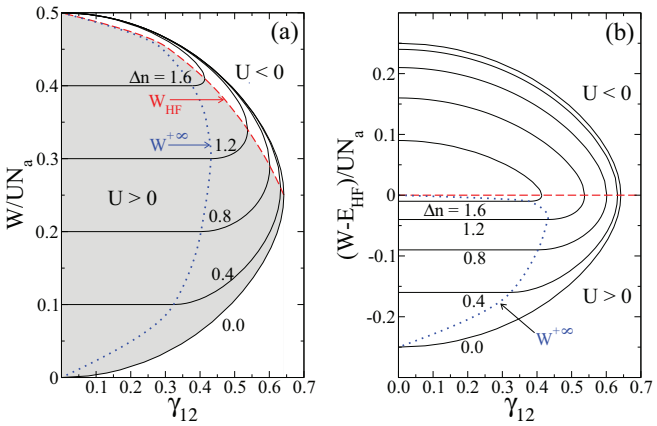

FIG. 2. (Color online) (a) Interaction energy W and (b) correlation energy $E_c = W - E_{\rm HF}$ of the attractive ($U < 0$) and repulsive ($U > 0$) Hubbard model as a function of the NN bond order γ_{12}, for representative charge transfers $\Delta n = \gamma_{22} - \gamma_{11}$. Exact results are given for rings having $N_a = 14$ sites and band filling $n = 1$. Repulsive (attractive) interactions correspond to the shaded (nonshaded) area in (a) and to negative (positive) values of E_c/U in (b). The red dashed curves indicate the Hartree-Fock energy $E_{\rm HF}$ corresponding to the largest representable value of γ_{12} for the given Δn. The dotted curves refer to the strongly correlated repulsive limit, i.e., to the largest representable γ_{12} allowing a minimal number of double occupations.

the bond order γ_{12}^0, which corresponds to an uncorrelated state. γ_{12}^0 decreases monotonously as Δn increases, vanishing in the strongly ionic limit $\Delta n = 2$. These changes in the representability range of γ_{12} versus $\Delta n = \gamma_{11} - \gamma_{22}$ are an important part of the functional dependence of W. They reflect the interplay between charge transfer and electron delocalization in the absence of interactions. (ii) For the uncorrelated upper bound γ_{12}^0 of γ_{12}, W coincides with the Hartree-Fock energy $E_{\rm HF} = UN_a[1 + (\Delta n/2)^2]/4$ since the electronic state yielding the largest γ_{12} is a Slater determinant: $W[\gamma_{12}^0, \Delta n] = W^0 = E_{\rm HF}$ for all Δn. Moreover, one observes that $\partial W/\partial\gamma_{12} \to +\infty$ for $\gamma_{12} \to \gamma_{12}^0$. This is a necessary condition in order that the ground-state density matrix satisfies $\gamma_{12}^{gs} < \gamma_{12}^0$ for arbitrary small values of $|U| > 0$, as expected from perturbation theory. (iii) Starting from γ_{12}^0, W decreases with decreasing γ_{12} reaching its lowest possible value W^∞ in the strongly correlated limit $\gamma_{12} = \gamma_{12}^\infty$, where all available electrons form pairs (N_e even). The decrease of W with decreasing γ_{12} means that the energy reduction $E_c = W - E_{\rm HF}$ associated to correlations is achieved at the expense of electron delocalization. Notice that the decrease of W is equivalent to an increase of the average number of double occupations $\omega = W/UN_a$. (iv) The strongly correlated limit is characterized by $W^\infty = UN_e/2$ and $\gamma_{12}^\infty = 0$, for finite systems with N_e even or in the thermodynamic limit. For N_e odd, we have $W^\infty = U(N_e - 1)/2$ and a nonvanishing γ_{12}^∞, which results from the delocalization of an unpaired electron throughout the empty lattice sites. In this case, γ_{12}^∞ depends in a non-trivial way on the lattice structure and on the band filling. (v) As expected, the correlation energy $E_c = W - E_{\rm HF} < 0$ increases in absolute value as γ_{12} decreases [see Fig. 2(b)]. Except for very large Δn, the contribution of correlations to W is as important as the Hartree-Fock energy when γ_{12} is small. For example, for $\Delta n = 0$ we have $W^\infty = 2E_{\rm HF}$ and thus $|E_c/E_{\rm HF}| = 1$ for $\gamma_{12} = \gamma_{12}^\infty$. As Δn increases, $|E_c|$ decreases in general since the fermions are more localized on one sublattice and thus the average number of double occupations is larger already for $U = 0$. Notice that E_c and W are proportional to γ_{12}^2 for $\gamma_{12}^2 \to 0$. It is easy to see that this implies $\gamma_{\rm gs} \propto t/U$ for $|U|/t \to \infty$.

A number of fundamental differences and some similarities between $W[\gamma]$ for attractive and repulsive interactions become apparent from Fig. 2 (see also Fig. 2 of Ref. [19]). The representability domains and thus γ_{12}^0 are the same in both cases. Moreover, the corresponding noncorrelated interaction energies have the same absolute value for all Δn. However, as γ_{12} decreases, and particularly in the strongly correlated limits, the behaviors are quite different. For $U < 0$, W decreases monotonously with decreasing γ_{12}, reaching the minimum value W^∞ only for $\gamma_{12} = 0$ (N_e even). This is independent of band filling n and charge transfer Δn [see Fig. 2(a)]. In contrast, for $U > 0$ one observes that W decreases faster with decreasing γ_{12} reaching in most cases the minimum value $W^\infty = 0$ already at a finite γ_{12} (see Fig. 2 of Ref. [19]). This holds as soon as $n \neq 1$ or $\Delta n \neq 0$. Moreover, while W^∞ depends on Δn if $U > 0$, we have the same W^∞ for all charge transfers if $U < 0$: $W^\infty = N_e/2$ for N_e even and $W^\infty = (N_e - 1)/2$ for N_e odd. This is of course a consequence of the different types of correlations. Strong attractive interactions imply that all the electrons are localized in pairs (maximal double occupations). Once formed, these pairs can be distributed at will among the sublattices, according to the actual value of Δn. In the repulsive case, strong correlations impose minimal average number of double occupations, which depends on γ_{ii} for $\gamma_{ii} > 1$, and thus on Δn ($W^\infty = 1 - \Delta n/2$). In addition, for $n \neq 1$ or $\Delta n \neq 0$, a significant degree of electron delocalization (not simply proportional to $1/N_a$) is still possible, even under the constraint of minimal double occupations. Consequently, the minimal W^∞ can be reached at a nonvanishing γ_{12} if the interactions are repulsive [19].

In order to compare the functional dependence of W for different N_a and Δn it is useful to scale the different domains of representability $\gamma_{12}^\infty \leqslant \gamma_{12} \leqslant \gamma_{12}^0$ to a common range, and to scale W with respect to its Hartree-Fock and strongly correlated bounds $E_{\rm HF} = W^0$ and W^∞. In Figs. 3 and 4, we therefore show $w = (W - W^\infty)/(W^0 - W^\infty)$ as a function of $g_{12} = (\gamma_{12} - \gamma_{12}^\infty)/(\gamma_{12}^0 - \gamma_{12}^\infty)$ for a number of 1D rings having different sizes and charge transfers. Once appropriately scaled, the striking similarity of all the results is revealed (see Figs. 3 and 4). One concludes that the largest part of the dependence of W on γ_{12} and Δn can be ascribed to the domain of representability of γ_{ij}, as defined by its limiting values for weak and strong correlations. Hence, the relative change in the interaction energy w associated with a given change in the degree of delocalization g_{12} can be regarded as approximately independent of the system under study. A similar behavior has already been observed for repulsive interactions [11,19].

In Fig. 4, results for different Δn are compared by taking rings with $N_a = 14$ sites as representative examples. Again, the dependence of the scaled w on g_{12} are quantitatively very similar for all Δn. Notice in particular the results for weak and strong correlations and the overall shape in the crossover region. This is quite remarkable since the nature of

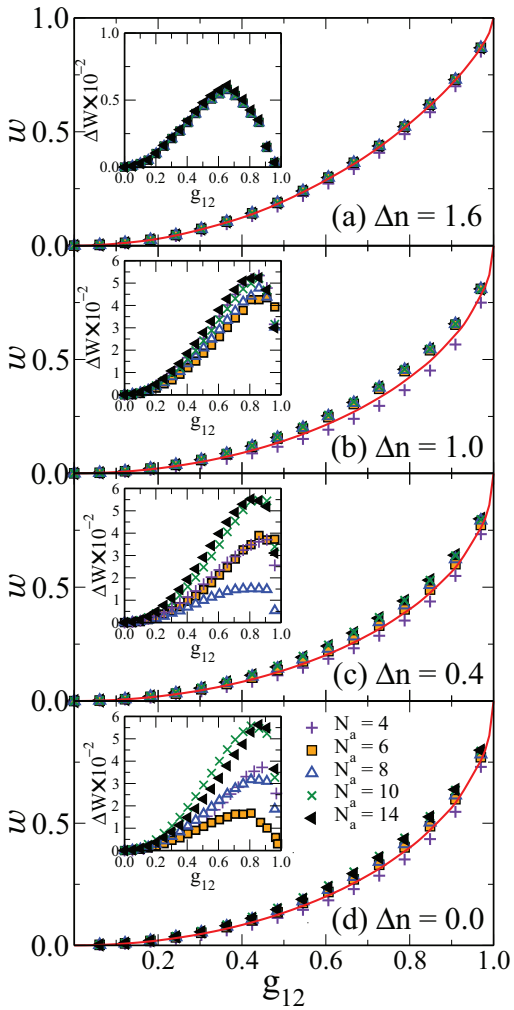

FIG. 3. (Color online) Scaled interaction energy $w = (W - W^\infty)/(W^0 - W^\infty)$ of the attractive Hubbard model as a function of the degree of electron delocalization $g_{12} = (\gamma_{12} - \gamma_{12}^\infty)/(\gamma_{12}^0 - \gamma_{12}^\infty)$. $W^0 = E_{\rm HF}$ and γ_{12}^0 refer to the uncorrelated limit, while W^∞ and γ_{12}^∞ to the strongly correlated limit. The symbols correspond to exact numerical results $W_{\rm ex}$ for rings having an even number of sites $N_a = 4$–14, half-band filling $n = 1$, and different charge transfers $\Delta n = \gamma_{11} - \gamma_{22}$. The curves are obtained using the dimer approximation $W_{\rm sc}$ [see Eq. (11)]. The inset figures highlight the relative errors $\Delta W = (W_{\rm sc} - W_{\rm ex})/(W^0 - W^\infty)$.

the electronic correlations changes significantly, from metallic to strongly ionic, as Δn is varied. A scaling hypothesis can be therefore applied to the interaction energy of the attractive Hubbard model, with good prospects of accuracy. In this way, it should be possible to transfer the functional dependence of W from simple to complex many-body problems, a strategy which has been most successful in DFT in the continuum [18,41].

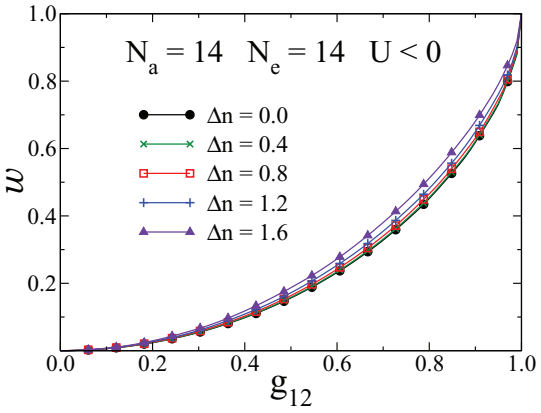

FIG. 4. (Color online) Charge-transfer dependence of the scaled interaction energy $w = (W - W^\infty)/(W^0 - W^\infty)$ of the attractive Hubbard model as a function of $g_{12} = (\gamma_{12} - \gamma_{12}^\infty)/(\gamma_{12}^0 - \gamma_{12}^\infty)$. Exact results are given for rings having $N_a = 14$ sites, band filling $n = 1$, and representative charge transfers $\Delta n = \gamma_{11} - \gamma_{22}$.

C. Dimer approximation to $W[\gamma]$

The numerical results of the previous subsection show that the interaction energy W of the attractive Hubbard model has very interesting scaling properties, as already observed in the repulsive model [11,12,19,20]. It is therefore useful to regard

$$w = \frac{W - W^\infty}{W^0 - W^\infty} \tag{9}$$

as a function of the degree of electron delocalization

$$g_{12} = \frac{\gamma_{12} - \gamma_{12}^\infty}{\gamma_{12}^0 - \gamma_{12}^\infty}. \tag{10}$$

Notice that the relation between w and g_{12} depends on γ_{ii}, and in particular on the charge transfer $\Delta n = \gamma_{22} - \gamma_{11}$ between sites. However, as shown in Fig. 4, this dependence is not very strong. A sound general approximation to W can then be obtained by scaling the known functional dependence of W corresponding to some model system. In order that the approach is practicable, the reference system must be simple enough to allow an analytic or numerically accurate calculation of $W[\gamma]$. In addition, it should be able to describe the fundamental physical interplay between electron delocalization, charge redistributions, and local interactions.

The Hubbard dimer is probably the simplest model that fulfills these conditions, as already demonstrated for the repulsive case [12,20]. We therefore propose the scaled dimer approximation

$$W_{\rm sc} = W^\infty + (W^0 - W^\infty)\frac{W_2 - W_2^\infty}{W_2^0 - W_2^\infty}, \tag{11}$$

where

$$W_2 = \frac{UN_a}{2}\left(1 - \frac{1}{2}\frac{g_{12}^2[1-(\Delta n/2)^2]\left\{1 - \sqrt{[1-(\Delta n/2)^2](1-g_{12}^2)}\right\}}{(\Delta n/2)^2 + g_{12}^2[1-(\Delta n/2)^2]}\right) \tag{12}$$

stands for the exact interaction-energy functional of the attractive Hubbard dimer ($U < 0$) with $N_e = 2$ electrons. In this case, $\gamma_{12}^0 = \sqrt{1-(\Delta n/2)^2}$ and $\gamma_{12}^\infty = 0$. It is easy to verify that Eqs. (11) and (12) reproduce the above-mentioned exact properties of $W[\gamma]$, which are common to all systems.

In order to quantify the validity of this approximation, we show in Fig. 3 results for W_{sc} as a function of g_{12} for various representative values of Δn and compare them with the corresponding exact calculations for rings having $N_a = 4$–10 ($n = 1$). One observes that W_{sc} follows quite closely the exact functional W_{ex} all along the crossover from weak to strong correlations for all charge transfers. This is quite remarkable taking into account the nontrivial dependence of the boundary values W^0, W^∞, γ_{12}^0, and γ_{12}^∞ on Δn and N_a. The quantitative discrepancies are in general small, as highlighted in the insets: $|W_{sc} - W_{ex}|/(W^0 - W^\infty) < 0.06$. They occur for relatively large values of γ_{12}, not very far from the weakly correlated regime, where the kinetic energy dominates. Consequently, a good performance of the dimer functional can be expected in the applications.

IV. RESULTS AND DISCUSSION

In this section, we apply the scaled dimer approximation to W in order to investigate the ground-state properties of the attractive Hubbard model in the framework of LDFT. We consider the Hamiltonian (1) with $U < 0$ on bipartite lattices having $\varepsilon_i = \varepsilon/2$ for sites i on sublattice $\mathcal{S}_1$ and $\varepsilon_i = -\varepsilon/2$ on sublattice $\mathcal{S}_2$. Finite rings having $N_a \leqslant 14$ sites are investigated together with the periodic 1D chain and 2D square lattice.

A. Ground-state properties

In Figs. 5–7, results are given for the ground-state properties of finite 1D rings, the 1D infinite chain, and the 2D square lattice as a function of the interaction strength $|U|/t$. Different values of the energy-level difference ε/t between the sublattices are considered at half-band filling. A number of general trends common to all these systems should be pointed out. The ground-state energy decreases with increasing $|U|/t$, approaching the limit $E_{gs}/N_a = (U-\varepsilon)n/2$ for $|U|/t \to \infty$ and N_e even. This corresponds to $N_e/2$ pairs of electrons occupying the most stable sublattice. In this case, all off-diagonal γ_{ij} vanish since the electrons are localized, and the average number of double occupations per site is maximal ($\omega = \omega^\infty = n/2$). The NN bond order γ_{12} and the associated kinetic energy decrease monotonously with increasing $|U|/t$. This contrasts with the behavior observed for repulsive interactions. In this case, γ_{12} shows a maximum as a function of U/t, when the value of U matches the difference between the sublattice levels (i.e., $U \simeq \varepsilon$) [20]. The charge transfer Δn and the average double occupations $\omega = W/UN_a$ increase with $|U|/t$. Notice, however, that there is no symmetry breaking in the homogeneous case ($\varepsilon = 0$) so that $\Delta n = 0$ for all U. Since this holds for both LDFT and exact results, the results for $\varepsilon = 0$ are omitted in part (b) of Figs. 5–7. For not too small ε, the system undergoes a qualitative change from a CDW ($\Delta n \simeq 0.9$–1.6 and $\gamma_{12} \simeq 0.3$–0.6) to a fully localized CDW ($\Delta n = 2$ and $\gamma_{12} = 0$) along the crossover

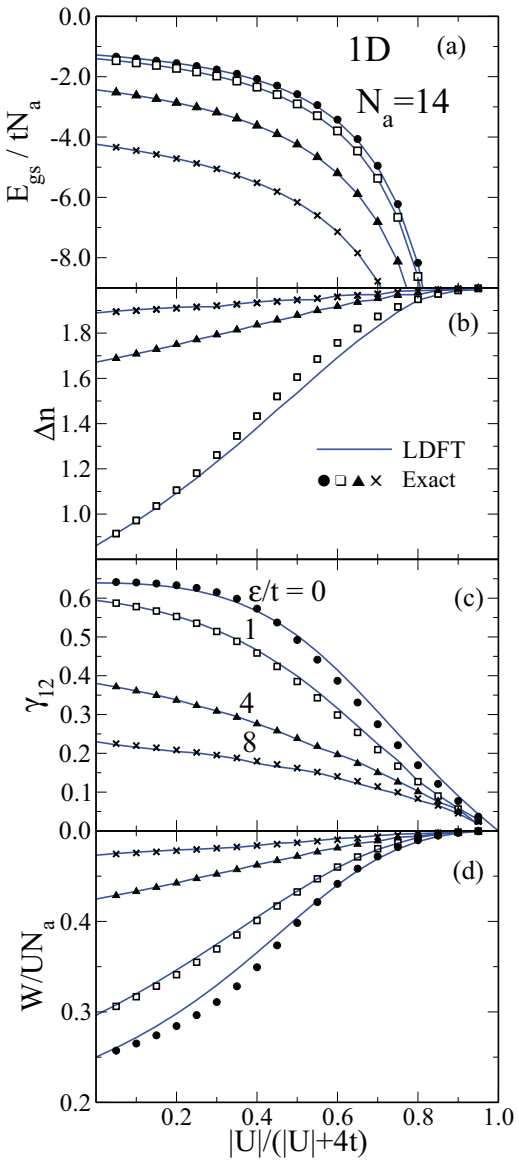

FIG. 5. (Color online) Ground-state properties of bipartite Hubbard rings having $U < 0$, $N_a = 14$, sites and half-band filling $n = 1$, as a function of the attractive interaction strength $|U|/t$. Different values of the energy-level shift ε between the sublattices are considered as indicated in (c). Results are given for (a) ground-state energy E_{gs}, (b) charge transfer $\Delta n = \gamma_{22} - \gamma_{11}$, (c) NN bond order γ_{12}, and (d) average number of double occupations per site W/UN_a. The symbols correspond to exact Lanczos diagonalizations and the solid curves to LDFT using the dimer approximation W_{sc} [see Eq. (11)].

from weak to strong correlations. One observes that Δn grows with increasing $|U|/t$ as the fermion pairs accommodate to the sublattice having the lowest single-particle energy [see parts (c) and (d) of Figs. 5–7].

The comparison between LDFT and exact numerical results obtained with the Lanczos and DMRG methods is most satisfactory (see Figs. 5 and 6). The considered ground-state properties are very well reproduced by the scaled dimer ansatz for all values of ε/t, not only close to the weakly and strongly correlated limits but also for intermediate interaction

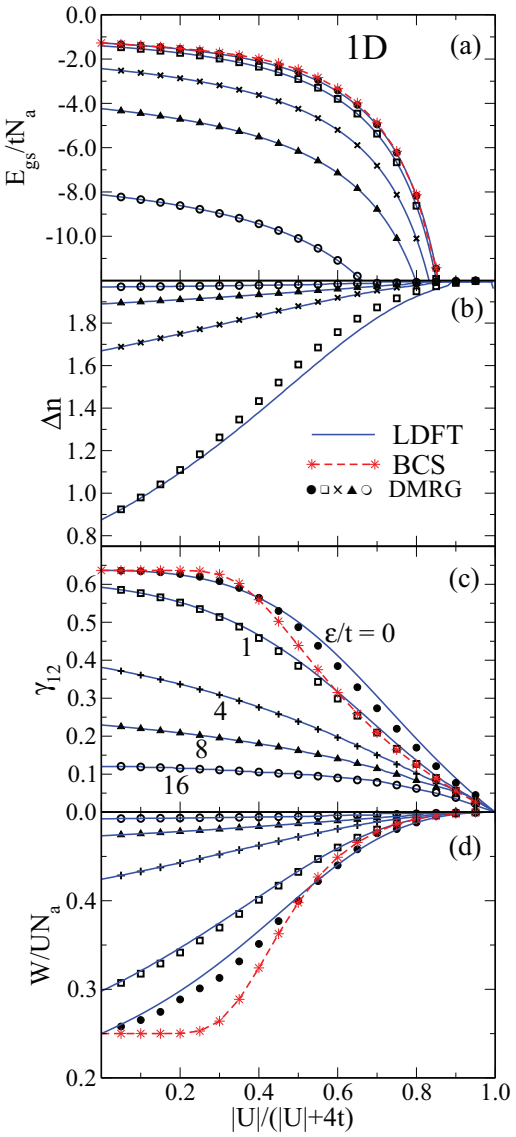

FIG. 6. (Color online) Ground-state properties of the one-dimensional attractive Hubbard model at half-band filling as a function of the interaction strength $|U|/t$. Different values of the alternating energy-level shift ε between the sublattices are considered as indicated in (c). Results are given for (a) ground-state energy $E_{\rm gs}$, (b) charge transfer $\Delta n = \gamma_{22} - \gamma_{11}$, (c) NN bond order γ_{12}, and (d) average number of double occupations per site W/UN_a. The solid curves correspond to LDFT using the scaling approximation $W_{\rm sc}$ [see Eq. (11)], the symbols to accurate numerical results obtained using the density-matrix renormalization-group method, and the red dashed curves with asterisks to the BCS approximation for $\varepsilon/t = 0$.

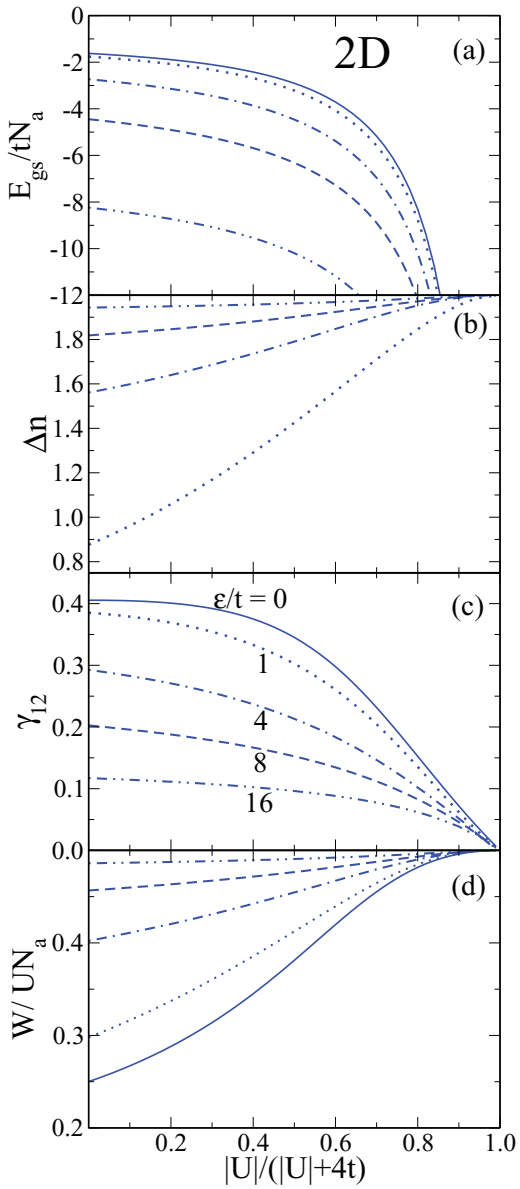

FIG. 7. (Color online) Ground-state properties of the two-dimensional attractive Hubbard model at half-band filling (square lattice) as a function of the interaction strength $|U|/t$. Results are given for (a) ground-state energy $E_{\rm gs}$, (b) charge transfer $\Delta n = \gamma_{22} - \gamma_{11}$, (c) NN bond order γ_{12}, and (d) average number of double occupations per site W/UN_a, as obtained by using LDFT and the scaling approximation $W_{\rm sc}$ [see Eq. (11)]. Different values of the energy-level shift ε between the sublattices are considered as indicated in (c).

strength. Moreover, the fact that γ_{12}, Δn, and W are all obtained with high precision shows that the LDFT results for $E_{\rm gs}$ are not the consequence of a strong compensation of errors. It is also interesting to note that the accuracy of the dimer ansatz actually improves as the charge distribution becomes more inhomogeneous, i.e., as ε/t and the CDW are stronger. This seems reasonable since larger values of ε enhance the importance of single-particle contributions to the energy, whose functional dependence is exactly known, and since large ε somehow tends to decouple the 1D chain in dimers, a limit for which correlations are taken into account exactly.

In Fig. 6, results are also given for the BCS approximation [4,5]. These were obtained for $\varepsilon/t = 0$ by solving the self-consistent equations in large finite rings and extrapolating to the infinite-chain limit. As shown in Fig. 6(a), the BCS approximation gives very accurate ground-state energies. Except for very minor overestimations for intermediate $|U|/t$, the BCS and exact results for $E_{\rm gs}$ are very difficult to tell apart.

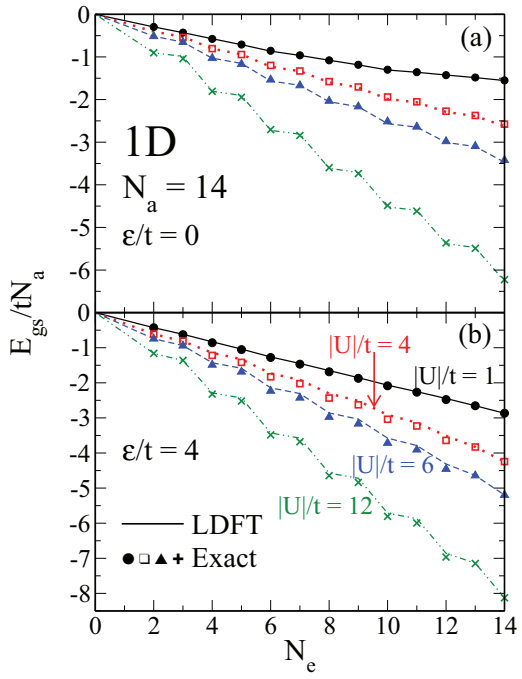

FIG. 8. (Color online) Ground-state energy of attractive Hubbard rings having $N_a = 14$ sites as a function of the number of electrons N_e. Different bipartite potentials ε and interaction strengths $|U|$ are considered. The symbols correspond to exact diagonalizations, while the solid lines connecting discrete points refer to LDFT with the scaled dimer functional W_{sc}.

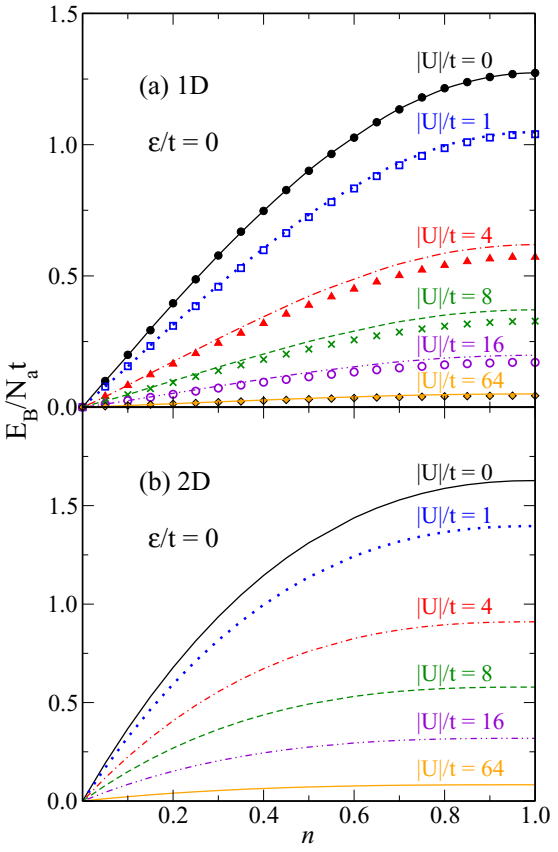

FIG. 9. (Color online) Binding energy per atom E_B/N_a of the (a) one-dimensional and (b) two-dimensional attractive Hubbard model as a function of band filling n. The curves are obtained by using LDFT with the scaled dimer functional W_{sc} for representative values of the interaction strength $|U|/t$. The symbols in (a) are the corresponding exact Bethe-ansatz results.

However, looking in more detail into the kinetic and interaction contributions, one finds that this good performance is the result of a significant compensation of errors [see Figs. 6(c) and 6(d)]. The average number of fermion pairs $\omega = W/UN_a$ is strongly underestimated for small $|U|/t$ and slightly overestimated for strong correlations. The bond order γ_{12} is correctly reproduced for small $|U|/t$ but it turns out to be too small for intermediate and strong coupling. The resulting underestimation of E_K for large $|U|/t$ is probably a consequence of the symmetry breaking involved in the mean-field BCS approach. Notice that the symmetry between the sublattices is not artificially broken in LDFT ($\varepsilon = 0$) and that the inaccuracies in E_K and W are much smaller than in the BCS approximation. As we shall see, this is important for the band-filling dependence of E_{gs} and for predicting the charge gap or pairing energy.

In Fig. 8, the band-filling dependence of the ground-state energy E_{gs} of rings having $N_a = 14$ sites and two different bipartite potentials ε/t is shown. For small $|U|/t$, one observes that E_{gs} decreases approximately linearly with N_e as the band is filled up ($n \leqslant 1$). The attractive interaction stabilizes the system through pair correlations. The same holds for the alternating potential $\pm\varepsilon/2$ since the pairs tend to occupy the lowest-energy sublattice. Moreover, the interaction leads to even-odd–like oscillations of E_{gs}, whose amplitude increases with $|U|/t$. This is a finite-size effect reflecting the changes in the number of fermion pairs as a function of N_e.

In Fig. 9, the binding energy per site $E_B/N_a = (U - \varepsilon/2)n - E_{gs}/N_a$ of the 1D chain and of the 2D square lattice are shown as a function of band filling n. The results were obtained by using LDFT for representative values of $|U|/t$. In the 1D case, the exact Bethe-ansatz results are also given for the sake of comparison [33,34]. Notice that electron-hole symmetry implies $E_B(n) = E_B(2-n)$, from which the results for $n > 1$ can be inferred. One observes that E_B increases monotonously with the number of carriers reaching its maximum at $n = 1$ for all $|U|/t$. Notice that $\partial E_B/\partial n$ is thus continuous for all n. The larger the attractive interaction is, the stronger is the localization of the fermions in pairs. Therefore, the binding decreases monotonously as $|U|/t$ increases, vanishing for all n in the strongly correlated limit. This behavior is qualitatively very different from what is observed in the repulsive model [34]. In this case, E_B shows a nonmonotonous band-filling dependence reaching its maximum at an intermediate n ($0 < n < 1$). Moreover, E_B remains finite even in the strongly correlated limit. Only for $n = 1$ and $U \to +\infty$ one finds $E_B = 0$.

A number of qualitative differences between attractive and repulsive interactions deserve to be discussed. In the repulsive case, one finds that E_B is essentially independent of U/t for small band fillings ($n \leqslant 0.2$) [34]. This implies that electron correlations can reduce most effectively the number of double occupation and the effects of the repulsive interactions if the carrier density is low. In contrast, in the attractive case $\partial E_B/\partial n$

depends significantly on $|U|/t$ for small n since pairs are formed even for very small n. In order that the binding can be effective, the electrons need to delocalize and pairs need to be broken. Therefore, E_B decreases strongly with increasing $|U|/t$, even at very low carrier densities. A further important difference is the nonmonotonous band-filling dependence of E_B for $U > 0$, which shows a maximum at an intermediate n ($0 < n < 1$) and a discontinuous $\partial E_B/\partial n$ for $n = 1$ [34]. In addition, we know that E_B remains finite in the limit of $U/t \to +\infty$, except if $n = 1$, while $E_B = 0$ for all n when $U/t \to -\infty$. This implies that some degree of electron delocalization can always be achieved, even under the constraint of vanishing number of double occupations ($n \neq 1$). In contrast, for $U < 0$ binding implies breaking pairs and overcoming an energy gap of the order of $|U|$, which becomes impossible in the strongly correlated limit.

The results obtained for 1D and 2D lattices are qualitatively similar. The comparison between LDFT and the exact solution of the 1D model is quite satisfactory in all regimes. The scaled dimer approximation is extremely good for weak and strong correlations for all n. In the crossover region, the results are also quite accurate, except for the largest carrier densities (see Fig. 9). The deviations found mainly at half-band filling for intermediate $|U|/t$ are relatively small. We therefore expect that the results obtained for the 2D square lattice are reliable.

B. Pairing energy

In order to quantify the stability of electron pair formation as a function of the model parameters, we consider the pairing energy

$$\Delta E_p(N_e) = E(N_e + 2) + E(N_e) - 2E(N_e + 1)\,, \quad (13)$$

which measures the energy change involved in transferring an electron from a $(N_e + 1)$-fermion system to another $(N_e + 1)$ system on N_a sites. Negative (positive) values of ΔE_p indicate that the $(N_e + 1)$ system is unstable (stable) with respect to such a fermion transfer. The charge gap $\Delta E_c(N_e) = E(N_e + 1) + E(N_e - 1) - 2E(N_e)$, usually considered in the context of repulsive interactions, and ΔE_p are simply related by $\Delta E_c(N_e) = \Delta E_p(N_e - 1)$.

In Fig. 10, the pairing energy in a 1D Hubbard ring having $N_a = 14$ sites is given as a function of the number of electrons N_e, for representative values of $|U|/t$ and ε/t. One observes important even-odd oscillations of ΔE_p as a function of N_e, which amplitude increases with increasing interaction strength. These systems are stable for N_e even ($\Delta E_p < 0$) whereas they are unstable, roughly by about the same absolute energy difference if $|U|/t$ is not too small, for N_e odd. The even-odd oscillations can be qualitatively explained by counting the total number of fermion pairs. For N_e even, the number of pairs that can be formed with $N_e + 2$ and N_e fermions is one more than twice the number of pairs in a $(N_e + 1)$ system. The former is $N_e + 1$ and the latter is N_e. The value of $\Delta E_p < 0$ gives a measure of the energy gained in the formation of this extra pair, which justifies denoting ΔE_p as pairing energy. In contrast, for N_e odd, one actually breaks a pair by transferring a fermion from one $N_e + 1$ system to the other. $N_e + 1$ (N_e) pairs can be formed before (after) transferring the fermion. Therefore, the changes

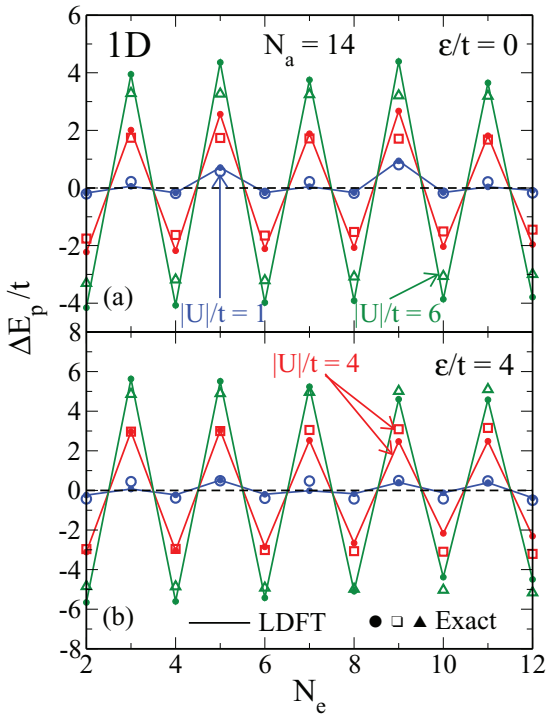

FIG. 10. (Color online) Pairing energy ΔE_p as a function of the number of electrons N_e in 1D attractive Hubbard rings having $N_a = 14$ sites. The symbols refer to exact Lanczos diagonalizations and the solid lines connecting small dots to LDFT with the scaled dimer functional. Representative values of the interaction strength $|U|$ and bipartite potential ε are considered.

of sign of ΔE_p do not correspond to any fundamental change in physical behavior but rather confirm the stability of pair formation for all band fillings, as one certainly expects at least in the limit of large ring sizes. It is thus more appropriate to regard $-\Delta E_p$ as the energy change associated to forming an extra pair for N_e odd. Notice that $|\Delta E_p|$ is systematically smaller than $|U|$, the limit of $|\Delta E_p|$ for $t = 0$. This difference measures the contribution of the kinetic energy to the pairing energy, which always tends to destabilize pair formation. Adding an alternating single-particle potential, for example $\varepsilon/t = 4$, enhances the value of $|\Delta E_p|$ and the amplitude of the even-odd oscillations since it singles out a more stable sublattice where the pairs are preferentially formed [compare Figs. 10(a) and 10(b)].

As already observed in Ref. [5], more subtle, so-called super-odd effects are found when $|U|/t$ is small. For example, for $|U|/t = 1$, one observes that ΔE_p is much larger at $N_e = 5$ and $N_e = 9$ than at the other odd numbers of electrons (see Fig. 10). This behavior, which is also present in the repulsive case [20], disappears for $|U|/t > 4$. It is a consequence of the specific single-particle spectrum of the rings [5]. Increasing ε/t tends to reduce the super-odd effects without suppressing them completely.

LDFT with the dimer ansatz for W reproduces very accurately the above-described behavior in good quantitative agreement with the exact results. The largest discrepancies are found for $N_e = 4m + 1$ with m integer and $|U|/t \geqslant 4$, where the LDFT results for ΔE_p are sometimes about 30%

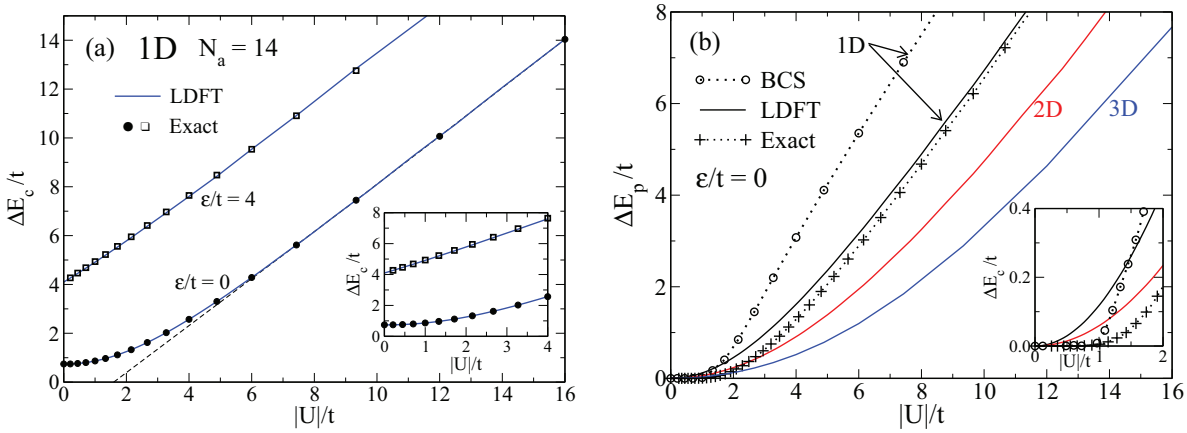

FIG. 11. (Color online) Pairing energy ΔE_p as a function of the interaction strength $|U|/t$ for the attractive Hubbard model on (a) rings having $N_a = 14$ sites and (b) the 1D chain, 2D square lattice, and 3D simple-cubic lattice. The solid curves correspond to LDFT with the scaled dimer functional. In (a) the symbols are exact numerical results. In (b) the crosses refer to the exact Bethe-ansatz solution and the open circles to the BCS approximation (1D). In the insets, small values of $|U|/t$ are highlighted.

too large. One also observes that LDFT tends to overestimate the super-odd effect for large $|U|/t$. As in the case of the ground-state properties, the accuracy of the dimer ansatz improves with increasing bipartite potential ε.

In Fig. 11, the pairing energies ΔE_p of half-filled 1D, 2D, and 3D lattices are shown as a function of the interaction strength $|U|/t$. The LDFT calculations are compared with exact numerical results for finite rings (Lanczos diagonalization for $N_a = 14$) and with the Bethe-ansatz solution and the BCS approximation of the homogeneous 1D chain. One observes that LDFT reproduces qualitatively very well the increase of ΔE_p as a function of $|U|/t$, as well as the value in the uncorrelated limit. In the presence of a finite bipartite potential (e.g., $\varepsilon/t = 4$), the results are remarkably accurate for all U/t. Nevertheless, LDFT overestimates ΔE_p systematically for homogeneous lattices (i.e., $\varepsilon/t = 0$). In particular, for the weakly correlated limit the predicted $|U|/t$ dependence is qualitatively different from the exact behavior. In the 1D chain, we obtain $\Delta E_p^{\mathrm{LDFT}} \propto (U/t)^2$ for $|U|/t \ll 1$, while the Bethe-ansatz solution yields $\Delta E_p^{\mathrm{BA}} = (4/\pi)\sqrt{|U|t}\exp(2\pi t/U)$ [4,34]. This is most probably a consequence of the local character of the dimer ansatz, which does take into account long-range correlation effects. These contributions, which are expected to be important for weak interactions, are best described from a k-space perspective. Indeed, the mean-field BCS approximation yields [4] $\Delta E_p^{\mathrm{BCS}} = 8t\exp(2\pi t/U)$, and is therefore much more accurate than LDFT for small $|U|/t$ [see the inset of Fig. 11(b)]. However, as $|U|/t$ increases, the formation of strongly correlated local pairs dominates. The BCS approach fails and the scaled dimer approximation becomes remarkably accurate [see Fig. 11(b) for $|U|/t \geqslant 2$]. The limitations of the BCS approach can be traced back to the already observed inaccuracies in the BCS kinetic and correlation energies (see Fig. 5).

The comparison between LDFT and exact results for the 1D chain allows us to estimate the reliability of our predictions on ΔE_p for the 2D square lattice and the 3D simple cubic lattice, which are shown in Fig. 11(b). One observes that in 2D and 3D the pairing energy increases monotonously with $|U|/t$ in a qualitatively similar way as in the 1D case. For small $|U|/t$, we find $\Delta E_p \propto (U/t)^2$. This is most probably an overestimation since the dimer ansatz is known to have difficulties in describing long-range correlations in the weakly correlated limit. However, for strong interactions (large $|U|/t$), a high accuracy can be expected, at least as good as in 1D.

In order to investigate the role of the dimensionality of the lattice on the pairing energy, we determine ΔE_p on the Bethe lattice as a function of the coordination number z. In Fig. 12, the LDFT results obtained using the scaled dimer ansatz are shown for band filling $n = 1$ and representative values of $|U|/t$. One observes that ΔE_p decreases with increasing z as the bandwidth $W = 4t\sqrt{z-1}$ increases. In fact, if one would scale the NN hopping integral t keeping W constant, the calculated ΔE_p would be nearly independent of z in the scaled dimer approximation since the parameters defining the interaction-energy functional would not be affected by changes

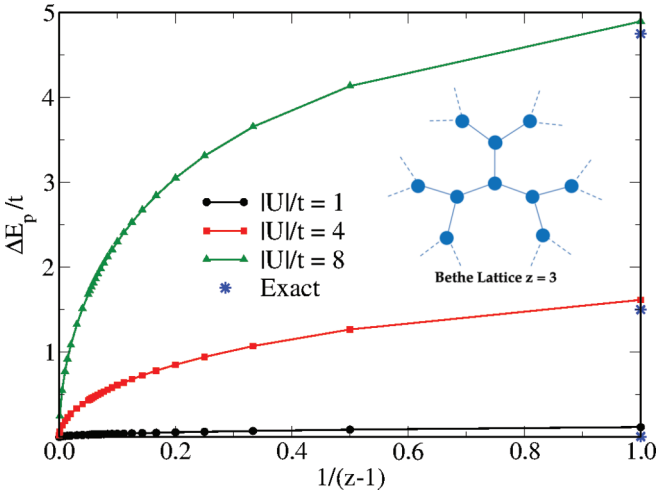

FIG. 12. (Color online) Pairing energy ΔE_p of the half-filled attractive Hubbard model on a Bethe lattice as a function of $1/(z-1)$, where z is the local coordination number (see inset).

in z. Concerning the dependence on $|U|/t$, we find a monotonic increase of ΔE_p with increasing interaction strength, which is very similar to the one observed in 1D, 2D, and 3D lattices (see also Fig. 11).

V. CONCLUSION

The attractive Hubbard model has been investigated in the framework of lattice density-functional theory by using the single-particle density matrix γ as the basic variable of the many-body problem. Once the transferability and scalability of the interaction-energy functional $W[\gamma]$ have been appraised, a simple approximation to W has been proposed, which is based on exact analytical solution of the attractive Hubbard dimer. In this way, a unified description of the interplay between electronic correlations, delocalization, and charge redistributions has been achieved, which covers the complete model-parameter range from weak to strong coupling and for all band fillings. Several important ground-state properties of the attractive Hubbard model on finite and infinite 1D, 2D, and 3D lattices have been determined by using this approximation. The limit of infinite dimensions has also been explored in the framework of the Bethe lattice. This includes the ground-state kinetic, Coulomb, and total energies, density distribution, nearest-neighbor bond orders, as well as the energy involved in pair formation. Comparisons with available exact results show that the present density-matrix functional approach yields in general a good qualitative and quantitative description of strongly correlated locally attracting fermions. Nevertheless, some quantitative limitations have been observed concerning the pairing energy ΔE_p in the limit of weak correlations. In this case, the present theory fails to reproduce the observed exponential dependence of ΔE_p on t/U and is outperformed by the mean-field BCS approximation. It has been argued that this is a consequence of the approximation to $W[\gamma]$ which, being based on a two-site problem, fails to incorporate long-range (small-k) correlation effects. All the same, it is important to observe that the dimer functional always remains qualitatively correct. In particular, it yields very accurate results for intermediate and large interaction strengths ($|U|/t \geqslant 2$) regimes where mean-field breaks down.

This study extends the domain of applicability of LDFT to attractive local interactions. An alternative perspective to the interesting physics of attracting fermions has been provided, which demonstrates once again the power of the concepts of density-functional theory as a general approach to the quantum many-body problem. Strong local interactions cannot be accurately described by simple mean-field approaches. Still, the proposed approximation appears to be quite successful in this challenging regime. This has been achieved by taking advantage of the universality of the exact $W[\gamma]$, as stated by the formulations of Hohenberg-Kohn or Levy-Lieb [15–17]. In this way, it is possible to incorporate valuable information on the physics of attractive interactions into the crucial energy functionals, particularly concerning the limits of weak and strong correlations and the functional dependence derived from simpler reference systems.

As in the original DFT of the inhomogeneous electron gas, the universality and flexibility of LDFT should be exploited to derive other approximations to the elusive interaction-energy functional. The limitations found in this work concerning the pairing energy indicate that a much better job could be done in the weakly correlated limit. This is likely to require a change of perspective, from the present local approach (so appealing in view of strong correlations and applications to low-symmetry systems) to a reciprocal space approach. Another route to further developments would be to incorporate information on the functional dependence of W for γ close to γ^0, which can be derived by using perturbation theory or by considering other reference systems.

ACKNOWLEDGMENTS

It is a pleasure to thank Dr. R. López Sandoval and Dr. M.-B. Lepetit for helpful discussions and suggestions at the early stages of this work. Computer resources provided by the IT Service Center of the University of Kassel and by the CSC of the University of Frankfurt are gratefully acknowledged.

[1] J. Bardeen, L. N. Cooper, and J. R. Scrieffer, Phys. Rev. **108**, 1175 (1957).
[2] J. Hubbard, Proc. R. Soc. London, Ser. A **276**, 238 (1963); **281**, 401 (1964); J. Kanamori, Prog. Theor. Phys. **30**, 275 (1963); M. C. Gutzwiller, Phys. Rev. Lett. **10**, 159 (1963).
[3] J. E. Hirsch and D. J. Scalapino, Phys. Rev. B **32**, 117 (1985); Phys. Rev. Lett. **56**, 2732 (1986); R. T. Scalettar, E. Y. Loh, J. E. Gubernatis, A. Moreo, S. R. White, D. J. Scalapino, R. L. Sugar, and E. Dagotto, *ibid.* **62**, 1407 (1989); T. Paiva, R. R. dos Santos, R. T. Scalettar, and P. J. H. Denteneer, Phys. Rev. B **69**, 184501 (2004).
[4] F. Marsiglio, Phys. Rev. B **55**, 575 (1997).
[5] K. Tanaka and F. Marsiglio, Phys. Rev. B **60**, 3508 (1999).
[6] N. Salwen, S. A. Sheets, and S. R. Cotanch, Phys. Rev. B **70**, 064511 (2004).
[7] J.-H. Hu, J.-J. Wang, G. Xianlong, M. Okumura, R. Igarashi, S. Yamada, and M. Machida, Phys. Rev. B **82**, 014202 (2010).
[8] B. Sacépé, T. Dubouchet, C. Chapelier, M. Sanquer, M. Ovadia, D. Shahar, M. Feigel'man, and L. Ioffe, Nat. Phys. **7**, 239 (2011).
[9] M. Ma and P. A. Lee, Phys. Rev. B **32**, 5658 (1985).
[10] A. Ghosal, M. Randeria, and N. Trivedi, Phys. Rev. B **65**, 014501 (2001); D. Valdez-Balderas and D. Stroud, *ibid.* **74**, 174506 (2006); T. A. Maier, G. Alvarez, M. Summers, and T. C. Schulthess, Phys. Rev. Lett. **104**, 247001 (2010); I. S. Burmistrov, I. V. Gornyi, and A. D. Mirlin, *ibid.* **108**, 017002 (2012).
[11] R. López-Sandoval and G. M. Pastor, Phys. Rev. B **61**, 1764 (2000).
[12] R. López-Sandoval and G. M. Pastor, Phys. Rev. B **66**, 155118 (2002).
[13] R. López-Sandoval and G. M. Pastor, Phys. Rev. B **67**, 035115 (2003).
[14] R. López-Sandoval and G. M. Pastor, Phys. Rev. B **69**, 085101 (2004).

[15] P. Hohenberg and W. Kohn, Phys. Rev. **136**, B864 (1964).
[16] W. Töws and G. M. Pastor, Phys. Rev. B **83**, 235101 (2011); **86**, 054443 (2012).
[17] M. Levy, Proc. Natl. Acad. Sci. USA **76**, 6062 (1979); E. H. Lieb, Int. J. Quantum Chem. **24**, 243 (1983); T. L. Gilbert, Phys. Rev. B **12**, 2111 (1975).
[18] W. Kohn and L. J. Sham, Phys. Rev. **140**, A1133 (1965).
[19] M. Saubanère and G. M. Pastor, Phys. Rev. B **79**, 235101 (2009).
[20] M. Saubanère and G. M. Pastor, Phys. Rev. B **84**, 035111 (2011).
[21] W. Töws, M. Saubanère, and G. M. Pastor, Theor. Chem. Acc. **133**, 1422 (2013).
[22] O. Gunnarsson and K. Schönhammer, Phys. Rev. Lett. **56**, 1968 (1986); A. Svane and O. Gunnarsson, Phys. Rev. B **37**, 9919 (1988).
[23] A. Schindlmayr and R. W. Godby, Phys. Rev. B **51**, 10427 (1995).
[24] K. Schönhammer, O. Gunnarsson, and R. M. Noack, Phys. Rev. B **52**, 2504 (1995).
[25] N. A. Lima, M. F. Silva, L. N. Oliveira, and K. Capelle, Phys. Rev. Lett. **90**, 146402 (2003).
[26] K. Capelle and V. L. Campo Jr., Phys. Rep. **528**, 91 (2013).
[27] C. Verdozzi, Phys. Rev. Lett. **101**, 166401 (2008).
[28] G. Stefanucci and S. Kurth, Phys. Rev. Lett. **107**, 216401 (2011).
[29] J. P. Bergfield, Z.-F. Liu, K. Burke, and C. A. Stafford, Phys. Rev. Lett. **108**, 066801 (2012).
[30] V. Brosco, Z.-J. Ying, and J. Lorenzana, Sci. Rep. **3**, 2172 (2013).
[31] A. E. Carlsson, Phys. Rev. B **56**, 12058 (1997).
[32] R. G. Hennig and A. E. Carlsson, Phys. Rev. B **63**, 115116 (2001).
[33] E. H. Lieb and F. Y. Wu, Phys. Rev. Lett. **20**, 1445 (1968).
[34] H. Shiba, Phys. Rev. B **6**, 930 (1972).
[35] E. H. Lieb, Phys. Rev. Lett. **62**, 1201 (1989).
[36] Y. Nagaoka, Solid State Commun. **3**, 409 (1965).
[37] H. Tasaki, Phys. Rev. B **40**, 9192 (1989).
[38] C. Lanczos, J. Res. Natl. Bur. Stand. **45**, 255 (1950); B. N. Parlett, *The Symmetric Eigenvalue Problem* (Prentice Hall, Engelwood Cliffs, NJ, 1980).
[39] S. R. White, Phys. Rev. Lett. **69**, 2863 (1992); Phys. Rev. B **48**, 10345 (1993).
[40] Notice that the present representability condition refers to the single-particle density matrix. This approach is different from the problem of the N-representability of the second-order reduced density matrix, which allows a direct calculation of W. See, for instance, A. J. Coleman, Rep. Math. Phys. **4**, 113 (1973).
[41] W. Kohn, Rev. Mod. Phys. **71**, 1253 (1999).